Electronic Supplementary Material (ESI) for Physical Chemistry Chemical Physics.

Supporting Information

Enhanced photoelectric performance of $Bi_2O_2Se/CuInP_2S_6$ heterojunction *via* ferroelectric polarization in two-dimensional $CuInP_2S_6$

Di Wang[1], Qiong Wu[1], Kaihan Shan[1], Mengwei Han[2], Wenyu Jiang[1], Weiting Meng[1], Yanqing Zhang[3], Weiming Xiong[1,a)]

[1]School of Physical Science & Technology, Guangxi University, Nanning 530004, China

[2]Radar NCO College, Air Force Early Warning Academy, Wuhan 430345, China

[3]School of Physics & Electronics, Nanning Normal University, Nanning 530004, China

[a)]Author to whom correspondence should be addressed: xiongwm3@gxu.edu.cn

I. I-V characteristics and photoelectric response of BOS/CIPS heterojunction under illumination of 405 and 650 nm

Figs. S1 and S2 show the I-V curves of $Bi_2O_2Se/CuInP_2S_6$ (BOS/CIPS) heterojunction under illumination of 405 and 650 nm, which are highly similar to those under other wavelengths shown in Figs. 3(a)-(c). The threshold voltage V_{th1} has a little change with the optical power intensity (OPI), and V_{th2} increases with the increase of OPI. The photocurrents I_{ph} increases with the increase of optical power intensity. The photoresponsivity (R), external quantum efficiency (EQE), and normalized detectivity (D^*) gradually decrease with the rise of OPI, which are similar to the rule of other wavelengths, indicating the broadband response properties of the heterojunction.

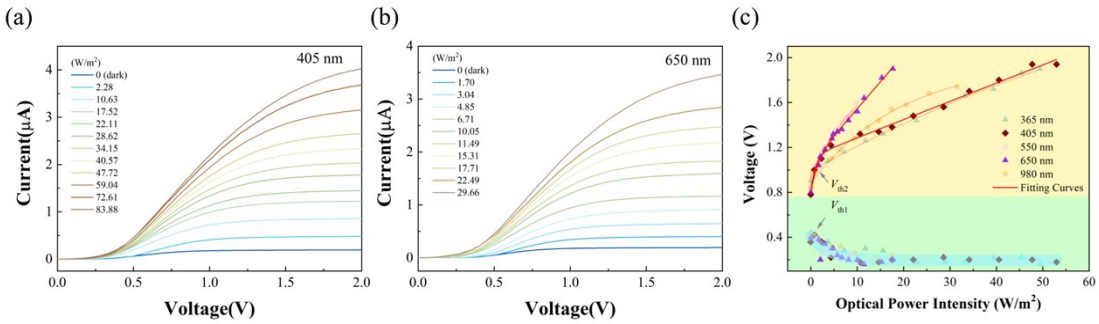

FIG. S1. *I-V* curves of BOS/CIPS heterojunction under various wavelengths of (a)405, (b) 650 nm and various OPIs. (c) Plots and fits of two threshold voltages (V_{th1} and V_{th2}) as functions of wavelength and OPI.

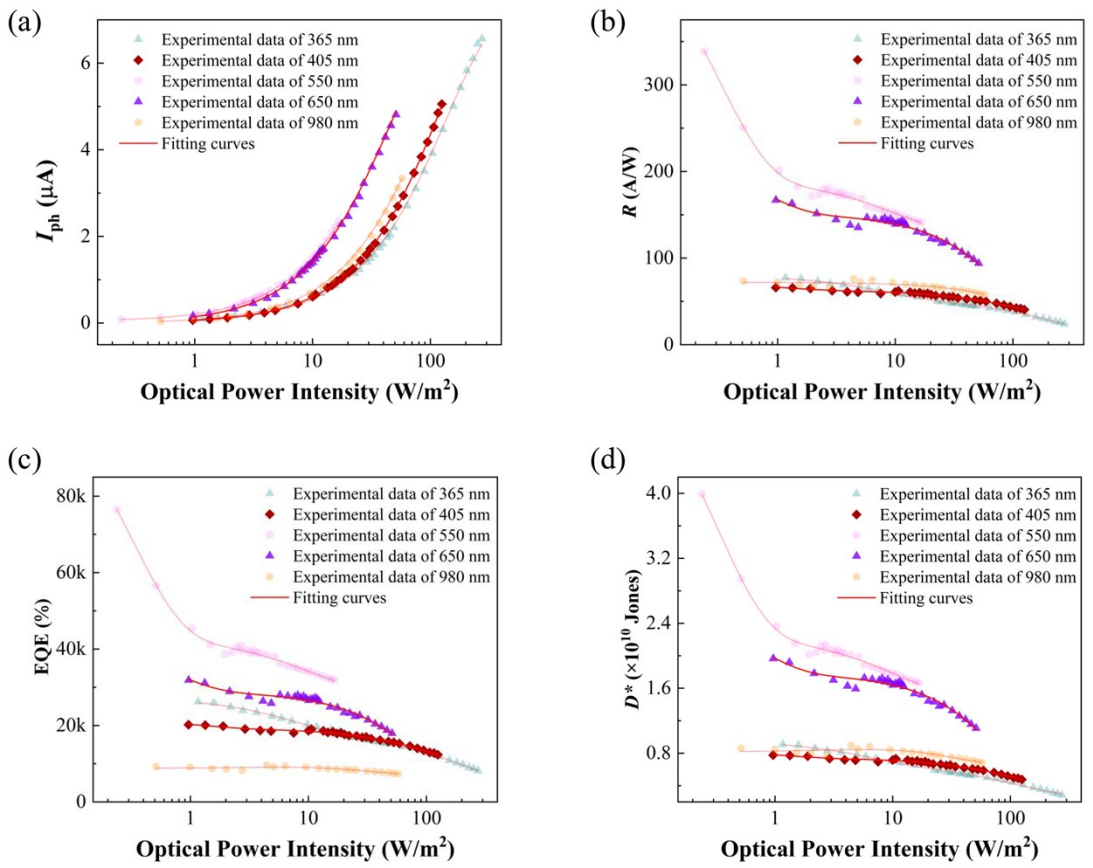

Fig. S2. (a) Photocurrents I_{ph}, (b) photoresponsivity R, (c) external quantum efficiency EQE, and (d) normalized detectivity D^* as functions of OPI. Experimental or calculated data of 365 (dark cyan triangle symbol), 405 (dark red diamond symbol), 550 (pink pentagon symbol), 650 nm (purple triangle symbol) and 980 nm (orange ball symbol) are plotted and fitted by red lines.

Figures S3(a) and S3(b) depict the current-voltage (I-V) characteristics of the photodetector under dark and illuminated conditions, respectively. These I-V curves exhibit three distinct regions with varying slopes. Specifically, stage I and III display a slope that is nearly zero, indicating a stable current response to the applied voltage, thereby facilitating the reliable operation of the photodetector. A comparison of Figs. S3(a) and S3(b) reveal a significantly larger slope in Stage II under the illuminated condition than that in the dark. This observation suggests that the current increases more rapidly with an increase in voltage under illumination, owing to the generation of photo-generated carriers.

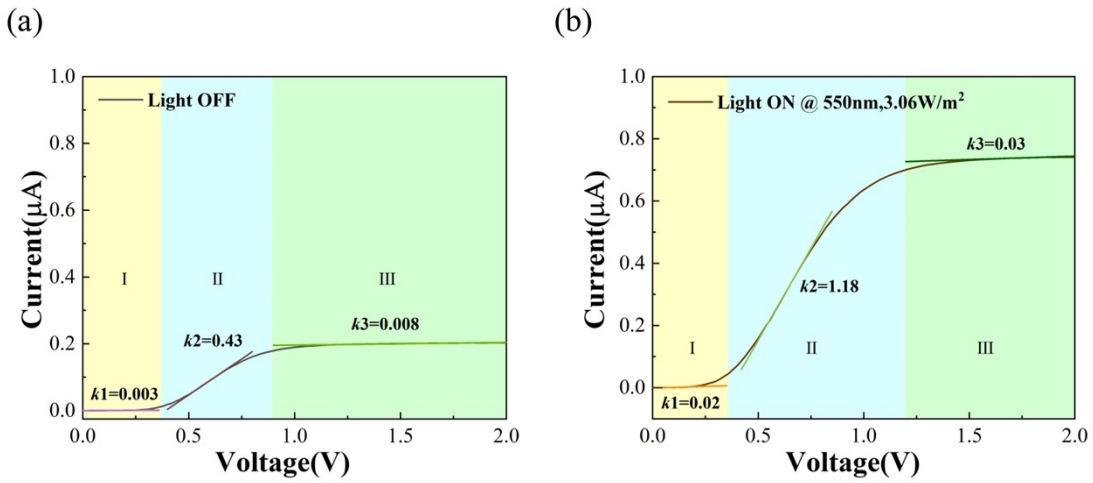

Fig. S3. The I-V curves at (a) dark and (b) 550nm, 3.06W/m^2 illumination are divided into three parts with different slopes.

II. High stability of BOS/CIPS heterojunction device

In the experiments, the I-V curves have been measured 5 times under a certain wavelength and OPI to ensure the stability and reliability of the data. Table S1 presents some selected measured current values and the corresponding calculated statistical parameters (i.e., average value $\bar{I}$, standard deviation σ, and relative standard deviation (RSD)) at a wavelength of 550nm and an irradiance of 3.06W/m^2, within the voltage scaning from 0 to 2V. Notably, the measured current values demonstrate a high degree of consistency, with standard deviations less than 4 nA. The relative standard deviation remains about 0.1% for voltages exceeding 0.6V. Correspondingly, the relationship of five-times-measured current and applied voltage have been plotted in Fig. S4. Curves measured for 5 times exhibited high levels of concordance, particularly at 2V. These results demonstrate the stability and repeatability of the photodetector.

Table S1. The selected current values were measured five times and the corresponding calculated average value $\bar{I}$, standard deviation σ, and relative standard deviation (RSD) under 550nm and 3.06W/m^2 illumination.

V (V)	I_1 (nA)	I_2 (nA)	I_3 (nA)	I_4 (nA)	I_5 (nA)	$\bar{I}$ (nA)	σ (nA)	RSD (%)
0.00	0.2281	0.2196	0.1511	0.1610	0.1558	0.1831	0.0335	18.2946
0.06	0.6237	0.6501	0.4782	0.4739	0.4577	0.5367	0.0825	15.3712
0.12	1.8000	1.8681	1.3900	1.3375	1.4093	1.5610	0.2252	14.4298

0.18	4.9959	5.3417	4.0583	4.1098	4.1485	4.5308	0.5330	11.7644
0.24	13.7446	13.7192	10.7161	11.7374	12.0146	12.3864	1.1807	9.5324
0.30	32.9218	33.6766	27.1365	26.5100	28.0303	29.6551	3.0239	10.1968
0.36	62.0129	62.7452	55.7492	54.0928	55.3473	57.9895	3.6329	6.2647
0.42	104.0159	107.1703	98.5818	96.5704	98.9249	101.0527	3.9225	3.8816
0.48	160.1877	161.7946	154.3476	154.1777	154.7498	157.0515	3.2619	2.0770
0.54	228.7337	227.9851	223.5737	221.6965	226.0608	225.6100	2.6482	1.1738
0.60	301.6194	306.8333	302.2289	298.5077	303.1489	302.4676	2.6826	0.8869
0.66	381.4926	384.4714	382.1544	377.1957	380.2666	381.1161	2.3903	0.6272
0.72	455.4261	456.6544	453.9902	454.5767	456.1223	455.3539	0.9747	0.2141
0.78	524.7431	525.4220	524.3500	524.5155	525.4701	524.9001	0.4631	0.0882
0.84	585.3696	585.8545	585.1053	587.0220	586.9404	586.0584	0.7913	0.1350
0.90	637.2689	637.7247	636.9621	638.1422	638.0479	637.6292	0.4522	0.0709
0.96	679.2213	680.9044	681.1229	681.7012	681.9225	680.9744	0.9516	0.1397
1.02	715.1856	715.3628	716.1440	718.0569	716.2884	716.2075	1.0187	0.1422
1.08	742.4905	742.6946	743.5920	744.8972	743.4018	743.4152	0.8488	0.1142
1.14	763.6580	764.7809	765.2733	766.6139	764.7927	765.0238	0.9559	0.1249
1.20	779.6771	780.6839	780.8485	782.4415	781.1490	780.9600	0.8905	0.1140
1.26	792.0071	792.4659	792.5610	794.5767	793.5358	793.0293	0.9201	0.1160
1.32	801.0172	801.6792	801.7651	804.2223	802.7778	802.2923	1.1172	0.1392
1.38	808.3293	809.0630	809.0208	810.7916	809.2709	809.2951	0.8126	0.1004
1.44	813.2475	814.1890	814.0930	816.3831	814.8035	814.5432	1.0450	0.1283
1.50	816.8280	817.8629	818.1959	820.1122	818.7064	818.3411	1.0779	0.1317
1.56	819.8415	821.7394	821.5950	823.2996	821.3850	821.5721	1.0993	0.1338
1.62	822.7154	823.8956	824.1216	824.7744	824.3156	823.9645	0.6883	0.0835
1.68	824.5248	826.1617	825.6666	827.0808	826.5914	826.0051	0.8754	0.1060
1.74	825.7967	828.4505	827.0266	828.5519	827.7585	827.5168	1.0198	0.1232
1.80	827.1638	829.3600	828.0329	829.9842	829.1449	828.7372	1.0080	0.1216
1.86	828.1862	830.2258	828.3671	830.5983	830.2241	829.5203	1.0261	0.1237
1.92	829.4080	830.8710	829.7317	831.1795	831.9730	830.6326	0.9449	0.1138
1.98	829.6399	831.9443	830.6080	832.1510	831.9274	831.2541	0.9754	0.1173
2.00	829.7683	832.3412	831.1345	832.2944	832.8989	831.6875	1.1182	0.1345

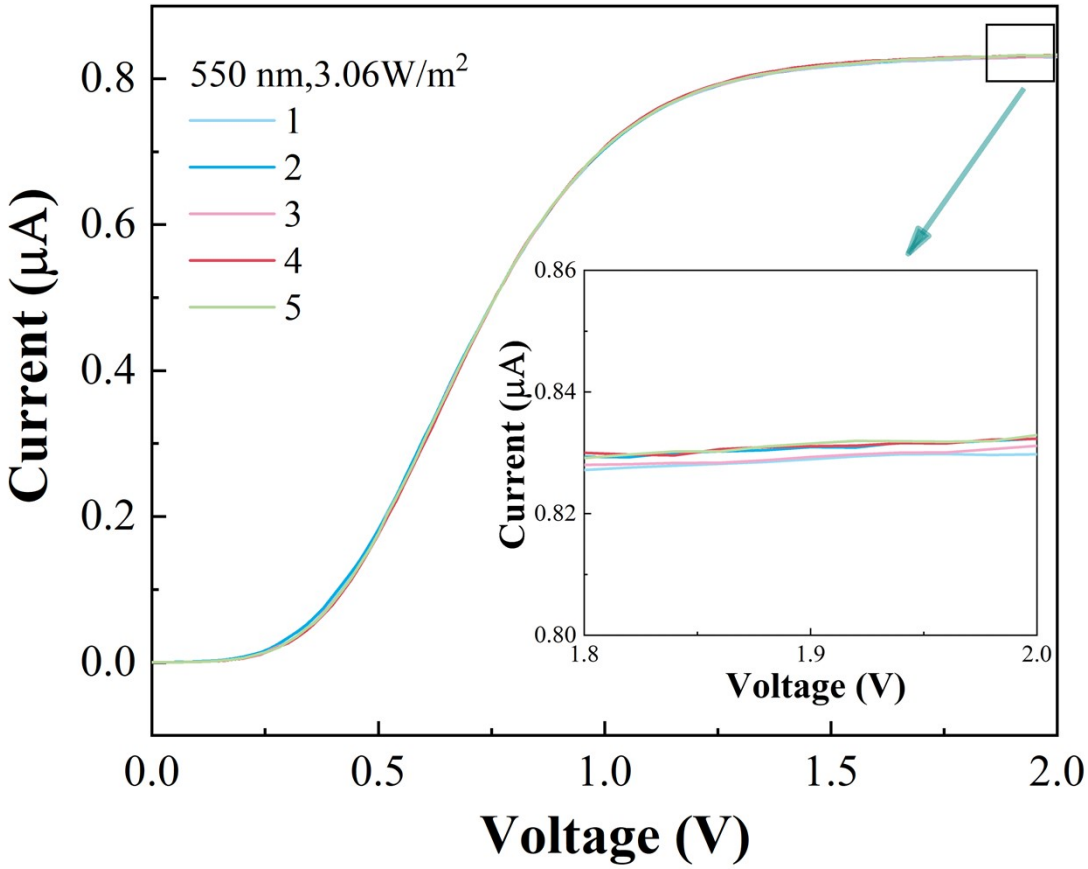

Fig. S4. I-V curves and locally enlarged images measured five times under 550 nm and 3.06 W/m^2 illumination.

III. The optical image of CVD-grown BOS nanosheets

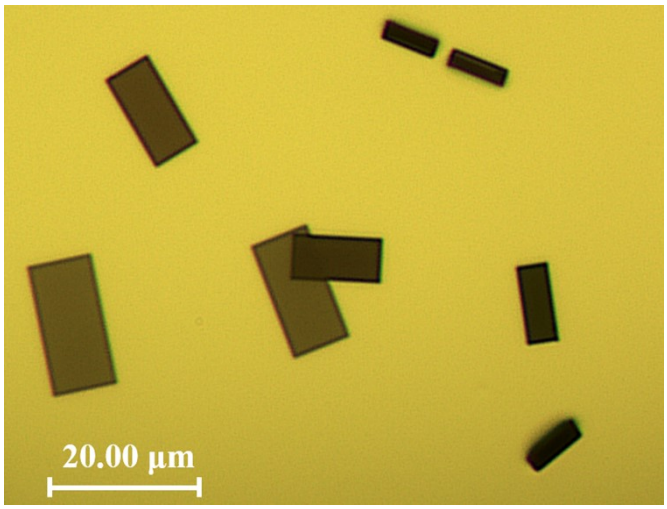

Fig. S5 BOS nanosheets grown on fluorophlogopite substrate

IV. Comparison of I-V characteristics of individual BOS and CIPS nanosheets and BOS/CIPS heterojunction

We focus on the electric responses of individual BOS and CIPS nanosheets and BOS/CIPS heterojunction. Electrodes are deposited on the BOS and CIPS to form the electric devices, as shown in Figs. S6a and S6b. Then, the I-V curves of BOS and CIPS nanosheets are measured. By comparing the I-V curves of CIPS, BOS and heterojunction, as shown in Figs. S6d-S6f, we can see that the I-V curves of heterojunction are asymmetrical and significantly different from those of the individual materials. For the BOS nanosheet, the current reaches 1.25 μA at 0.1 V in the dark, indicating its high carrier mobility. Under the light illumination condition, the current increases to about 3.6 μA at 0.1 V, demonstrating the excellent photoelectric response of BOS nanosheet. For the CIPS nanosheet, the I-V curve exhibits strong nonlinear and the nonzero current under zero applied voltage demonstrates the effect of ferroelectric polarization-induced built-in electric field on the I-V characteristics. For the BOS/CIPS heterojunction, we have obtained the I-V curves under dark and illuminated conditions, as shown in Fig. S6f.

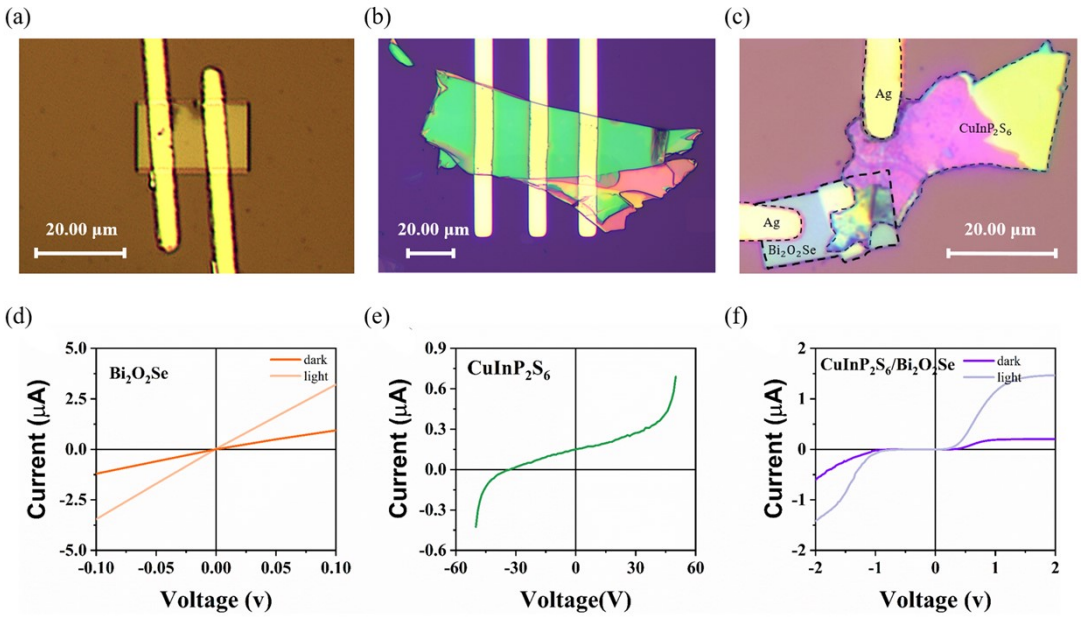

Fig. S6 Optical images of the test structures of individual (a) BOS (b) CIPS nanosheets and (c) BOS/CIPS heterojunction. Corresponding *I-V* characteristics of individual (d) BOS (e) CIPS nanosheets and (f) BOS/CIPS heterojunction

V. Influence of shot noise and 1/*f* noise on normalized detectivity D^*

Generally speaking, shot noise is caused by the dispersion of carriers, which is the main source of noise in most semiconductor devices. The formula of the shot noise current is $i_{shot} = \sqrt{2eI_{dark}\Delta f}$, where e is the electron charge, I_{dark} is the dark current of our device, Δf is the bandwidth. According to our measured data, the shot noise current is calculated to be 3.3×10^{-10} A for our device. Then, we can obtain the equivalent noise power by $P_{NEP} = i_{shot}/R$, where R is the photoresponsivity. If only shot noise is considered, the normalized detectivity can be written as $D^* = \sqrt{S\Delta f}/P_{NEP}$, this formula also can be written as $D^* = \frac{R}{\sqrt{\frac{2eI_{dark}}{S}}}$, which is consistent with the formula used in this work.[S1]

On the other hand, the 1/*f* noise is usually caused by local defects or trace impurities in the device, and is inversely proportional to the circuit frequency, mainly in the low-frequency domain below 1 kHz. If both 1/*f* noise and shot noise are considered, the root-mean-square noise current, *i.e.*, $i_n = \sqrt{\frac{\sum_1^N (I_i - \bar{I})^2}{N}}$, is calculated by measuring the time-dependent current of the device in the dark state under a certain applied voltage (i.e., 2V), as shown in **Tab. S2**. Then, the equivalent noise power is obtained by $P_{NEP} = i_n/R$. Finally, the D^* could be calculated by $D^* = \sqrt{S\Delta f}/P_{NEP}$. Considering the 1/*f* noise and shot noise, the calculated D^* is about 1.05×10^9 Jones at 550 nm, which is a little smaller than the one that the only shot noise is considered (2.81×10^9 Jones).

After referring to a large number of relevant literatures[S2-S11], we find that the normalized detectivity is generally calculated by $D^* = R/\sqrt{2eI_{dark}/S}$ and only the shot noise is considered in the calculation, as listed in **Tab. S2**. In order to have

comparability with the detector performance in previous works[11,15,26,27,40-42], we only consider the influence of shot noise on the value of D^* and the $1/f$ noise is neglected in this work.

Table S2
Time-dependent current data of devices in dark state at 2V

Time (s)	I_{dark} (A)	Time (s)	I_{dark} (A)	Time (s)	I_{dark} (A)
1.53350	3.40E-07	1.53566	3.45E-07	1.53782	3.43E-07
1.53357	3.41E-07	1.53573	3.43E-07	1.53788	3.46E-07
1.53363	3.40E-07	1.53579	3.44E-07	1.53795	3.43E-07
1.53370	3.41E-07	1.53586	3.42E-07	1.53802	3.42E-07
1.53376	3.43E-07	1.53592	3.43E-07	1.53808	3.44E-07
1.53383	3.42E-07	1.53599	3.44E-07	1.53815	3.45E-07
1.53389	3.41E-07	1.53605	3.42E-07	1.53821	3.42E-07
1.53396	3.41E-07	1.53612	3.43E-07	1.53828	3.44E-07
1.53402	3.40E-07	1.53618	3.42E-07	1.53834	3.42E-07
1.53409	3.41E-07	1.53625	3.44E-07	1.53841	3.43E-07
1.53415	3.44E-07	1.53631	3.44E-07	1.53848	3.44E-07
1.53422	3.41E-07	1.53638	3.43E-07	1.53854	3.43E-07
1.53428	3.41E-07	1.53644	3.43E-07	1.53861	3.43E-07
1.53435	3.41E-07	1.53651	3.43E-07	1.53867	3.42E-07
1.53441	3.42E-07	1.53658	3.42E-07	1.53874	3.43E-07
1.53448	3.42E-07	1.53664	3.45E-07	1.53880	3.45E-07
1.53455	3.43E-07	1.53671	3.42E-07	1.53887	3.43E-07
1.53461	3.42E-07	1.53677	3.44E-07	1.53893	3.42E-07
1.53468	3.42E-07	1.53684	3.45E-07	1.53900	3.43E-07
1.53474	3.45E-07	1.53691	3.44E-07	1.53906	3.42E-07
1.53481	3.43E-07	1.53697	3.44E-07	1.53913	3.46E-07
1.53488	3.43E-07	1.53704	3.43E-07	1.53920	3.43E-07
1.53494	3.42E-07	1.53710	3.42E-07	1.53926	3.42E-07
1.53500	3.43E-07	1.53717	3.43E-07	1.53933	3.43E-07
1.53507	3.47E-07	1.53723	3.45E-07	1.53939	3.45E-07
1.53513	3.43E-07	1.53730	3.43E-07	1.53946	3.44E-07
1.53520	3.43E-07	1.53736	3.43E-07	1.53952	3.42E-07
1.53527	3.42E-07	1.53743	3.43E-07	1.53959	3.43E-07
1.53533	3.43E-07	1.53749	3.42E-07	1.53965	3.42E-07
1.53540	3.46E-07	1.53756	3.46E-07	1.53972	3.43E-07
1.53546	3.43E-07	1.53762	3.43E-07	1.53978	3.44E-07
1.53553	3.42E-07	1.53769	3.44E-07	1.53985	3.42E-07
1.53559	3.44E-07	1.53775	3.42E-07	1.53991	3.43E-07

$$\bar{I} = \frac{\sum_{1}^{N} I_i}{N} = 3.43 \times 10^{-7} A$$

$$i_n = \sqrt{\frac{\sum_{1}^{N} (I_i - \bar{I})^2}{N}} = 1.31 \times 10^{-9} A$$

$$P_{NEP} = \frac{i_n}{R} = 3.87 \times 10^{-12} W \ (R = 338.94 A/W, @550nm)$$

$$D^* = \frac{\sqrt{S\Delta f}}{P_{NEP}} = 1.05 \times 10^9 \, Jones$$

References

S1. Q. Wang, Y. Zhang, and Z. Wei, *Chin. J. Chem.*, 2023, **41**, 958-978.

S2. L. Zeng, S. Lin, Z. Lou, H. Yuan, H. Long, Y. Li, W. Lu, S. Lau, D. Wu and Y. Tsang, *Asia Mater*, 2018, **10**, 352–362.

S3. L. Ye, H. Li, Z. Chen, and J. Xu, *ACS Photonics*, 2016, **3**(4), 692-699.

S4. D. Wu, C. Jia, F. Shi, L. Zeng, P. Lin, L. Dong, Z. Shi, Y. Tian, X. Lia and J. Jie, *J. Mater. Chem. A*, 2020, **8**, 3632-3642.

S5. C. Fang, J. Han, M. Yu, W. Liu, S. Gao and K. Huang, *Adv. Mater. Interfaces*, 2022, 9, 2102091.

S6. D. Qiu, P. Hou, J. Wang and X. Ouyang, *Appl. Phys. Lett.*, 2023, **123**, 111102.

S7. X. Liu, R. Li, C. Hong, G. Huang, D. Pan, Z. Ni, Y. Huang, X. Ren, Y. Cheng and W. Huang, *Nanoscale*, 2019, **11**, 20707–20714.

S8. Y. Chen, W. Ma, C. Tan, M. Luo, W. Zhou, N. Yao, H. Wang, L. Zhang, T. Xu, T. Tong, Y. Zhou, Y. Xu, C.Yu, C. Shan, H. Peng, F. Yue, P. Wang, Z. Huang and W. Hu, *Adv. Funct. Mater.*, 2021, **31**, 2009554.

S9. T. Yang, X. Li, L. Wang, Y. Liu, K. Chen, X. Yang, L. Liao, L. Dong and C. Shan, *J. Mater. Sci.*, 2019, **54**, 14742–14751.

S10. X. Liu, W. Wang, F. Yang, S. Feng, Z. Hu, J. Lu and Z. Ni, *Sci. China Inf. Sci.*, 2021, 64, 140404.

S11. M. Yang, X. Zhang, H. Zhou, G. Fu, X. Zhou, Y. Lian, J. Hao, H. Yu, X. Zhu and J. Wang, *J. Mater. Chem. C*, 2022, **10**, 15377-15385.